Interband optical transitions in GaAs-$Ga_{1-x}Al_xAs$ and InAs-GaSb superlattices

Yia-Chung Chang
Department of Physics and Materials Research Laboratory, University of Illinois at Urbana—Champaign, 1110 West Green Street, Urbana, Illinois 61801

J. N. Schulman*
Department of Physics and Astronomy, University of Hawaii at Manoa, Honolulu, Hawaii 96822
(Received 2 July 1984)

Optical properties of GaAs-$Ga_{1-x}Al_xAs$ and InAs-GaSb superlattices are studied within the framework of tight-binding approximation. The momentum matrix elements between tight-binding orbitals are related to those between Brillouin-zone-center Bloch states computed by a full-zone $\mathbf{k}\cdot\mathbf{p}$ theory. The optical matrix elements of transitions from several valence subbands to several conduction subbands are calculated as functions of the well width and of the wave vector. It is found that the mixing of the heavy- and light-hole components in the superlattice states gives rise to a large variation in the optical matrix elements as $\mathbf{k}$ moves away from the zone center. The band mixing in conjunction with the exciton effect leads to weak structures in the absorption spectrum which can account for the forbidden transitions observed in several recent experiments.

I. INTRODUCTION

Semiconductor superlattices or quantum wells have been studied extensively in recent years.[1–10] The optical properties (including photoabsorption, photoluminescence, and light scattering) of these materials, especially GaAs-$Ga_{1-x}Al_xAs$ multilayer structures, have been investigated experimentally by many groups.[10–14] Sai-Halasz *et al.*[10] have reported theoretical calculations on the absorption coefficient of semiconductor superlattices based on a simple envelope-function approximation (EFA). The EFA calculation is able to predict the general features of the absorption spectrum, but it cannot explain certain weak structures corresponding to the "forbidden" transitions.[11,12]

In this paper we report detailed theoretical calculations of the optical properties of semiconductor superlattices, based on a realistic tight-binding model. The interacting parameters in our tight-binding model are adjusted to reproduce the experimentally determined band gaps and the electron and hole effective masses. Both GaAs-$Ga_{1-x}Al_xAs$ and InAs-GaSb superlattices are considered. In the accompanying paper[15] (hereafter referred to as I) we demonstrated the importance of using a many-band tight-binding representation to describe the superlattice electronic states, particularly when they contain strong admixtures of several bulk bands. Although such mixing does not alter the superlattice energy levels appreciably (about 20%), it can sometimes lead to substantial modification of optical properties.

We have previously reported the effect of band mixing on the optical properties of GaAs-$Ga_{1-x}Al_xAs$ superlattices.[9] We found that the mixing of heavy-hole (HH) and light-hole (LH) bulk states in the superlattice valence subband states at the zone center can lead to a crossover behavior of the optical matrix elements as the well thickness is varied. We also speculated that the LH-HH mixing in superlattice valence subbands away from the zone center in conjunction with the exciton effect may account for the weak structure corresponding to the forbidden HH3-CB1 (CB is the conduction band) transition observed in several experimental spectra.[11–13]

In this paper, we extend the previous work to include the dependence of the optical matrix element on the wave vector ($\mathbf{k}$). We find that the optical matrix elements associated with various valence- to conduction-subband transitions are very sensitive to the variation of the wave vector in directions parallel to the interface ($\mathbf{k}_t$). This is a result of complicated band-mixing effects at $\mathbf{k}_t \neq 0$ in the valence-subband states. The same effect also causes the valence-subband energies of the superlattice to be rather complicated functions of $\mathbf{k}_t$. Both complications in the valence-band structures and optical matrix element have important effects on the photoabsorption of the superlattice. By including the exciton effect in a simple model, we are able to obtain a theoretical absorption spectrum of a superlattice in very good agreement with the experimentally measured spectrum. We confirm the previous speculation that the combination of band mixing and the exciton effect can give rise to a weak structure corresponding to the forbidden HH3-CB1 transition. In addition, we report theoretical studies on the optical properties of InAs-GaSb superlattices.

In Sec. II we describe the theoretical model used, giving the procedures for determining the momentum matrix elements between the tight-binding basis states and discuss the symmetry properties of the superlattice eigenstates as well as the selection rules for interband optical transitions in the superlattice. In Sec. III we discuss the resulting optical matrix elements squared for various valence to conduction-band transitions as functions of the well width and the parallel wave vector ($\mathbf{k}_t$) as well as the theoretically predicted photoabsorption spectra for some sample GaAs-$Ga_{1-x}Al_xAs$ and InAs-GaSb superlattices. In Sec. IV some concluding remarks are provided.

II. THEORY

The optical property of concern here is the photoabsorption of the semiconductor superlattice. The optical matrix elements studied here for absorption may also be used to analyze other optical properties, such as photoluminescence and photoconductivity.

The absorption coefficient of a superlattice is given by[16] (apart from a constant factor)

$$\alpha(\hbar\omega)=\frac{1}{\omega}\sum_{\mathbf{k}_t,q}\sum_{n',n}|\hat{\epsilon}\cdot\mathbf{P}_{nn'}(\mathbf{k}_t,q)|^2 \times\delta(E_{n'}(\mathbf{k}_t,q)-E_n(\mathbf{k}_t,q)-\hbar\omega)\ , \tag{1}$$

where $\hat{\epsilon}$ denotes the direction of polarization and $\mathbf{P}_{nn'}(\mathbf{k}_t,q)\equiv\langle n',\mathbf{k}_t,q\,|\,\mathbf{p}\,|\,n,\mathbf{k}_t,q\rangle$ denotes the momentum matrix element between superlattice eigenstates associated with the n'th and nth subbands. The symbols $\mathbf{k}_t$ and q designate the projections of the wave vector in the plane parallel to the interface and along the axis perpendicular to the interface, respectively, $E_n(\mathbf{k}_t,q)$ the energy associated with the eigenstate $|\,n,\mathbf{k}_t,q\,\rangle$.

To evaluate $\alpha(\hbar\omega)$ for a realistic superlattice, we need to know the detailed energy spectra and the momentum matrix elements between various electronic states. In the present calculation, we adopt a tight-binding method. The electronic eigenstates of a superlattice are expanded in terms of planar atomic orbitals, $\psi_\alpha(\mathbf{k}_t,l)$. These are two-dimensional Bloch sums of atomic orbitals in a plane parallel to the interface, where α denotes the orbital symmetry ($s,x,y,z,\ldots$) and l denotes the position of the atomic plane. The expansion can be written as

$$|\,n,\mathbf{k}_t,q\,\rangle=\sum_{\alpha,l}A_\alpha^n(\mathbf{k}_t,q,l)\,|\,\psi_\alpha(\mathbf{k}_t,l)\rangle\ , \tag{2}$$

where l runs over all atomic planes of the whole superlattice. The energy spectra $E_n(\mathbf{k}_t,q)$ and the expansion coefficients (also known as the envelope function) $A_\alpha^n(\mathbf{k}_t,q,l)$ can be obtained by the "reduced Hamiltonian" method as described in Ref. 17. The tight-binding model adopted here is identical to that of I. Five atomic orbitals (labeled with s^*, s, x, y, z) per atomic site are used.

A. Momentum matrix elements

The momentum matrix element $P_{nn'}(\mathbf{k}_t,q)$ can be written in terms of the coefficients $A_\alpha^n(\mathbf{k}_t,q,l)$ and the momentum matrix elements between planar atomic orbitals

$$\mathbf{P}_{nn'}(\mathbf{k}_t,q)=\sum_{\substack{\alpha,\alpha'\\ l,l'}}A_\alpha^{n*}(\mathbf{k}_t,q,l)A_{\alpha'}^{n'}(\mathbf{k}_t,q,l') \times\langle\psi_\alpha(\mathbf{k}_t,l)\,|\,\mathbf{p}\,|\,\psi_{\alpha'}(\mathbf{k}_t,l')\rangle\ . \tag{3}$$

In our tight-binding model, the atomic orbitals are sufficiently localized so that the momentum matrix elements between atoms separated by more than first-neighbor distance can be neglected. Furthermore, for the direct superlattice of interest here, the low-lying conduction subband states are almost purely s like and the valence subband states are almost purely p like. Therefore, the optical matrix elements involving transitions between two s-like orbitals or two p-like orbitals can be ignored. Furthermore, the transitions involving s^*-like orbitals are ignored. These considerations leave us with only four independent parameters to determine for each constituent material. These parameters are

$$\begin{aligned}
P_{aa}&=i\langle\phi_s(\tau_a)\,|\,p_x\,|\,\phi_x(\tau_a)\rangle(2/m_e)^{1/2}\ ,\\
P_{cc}&=i\langle\phi_s(\tau_c)\,|\,p_x\,|\,\phi_x(\tau_c)\rangle(2/m_e)^{1/2}\ ,\\
P_{ac}&=i\langle\phi_s(\tau_a)\,|\,p_x\,|\,\phi_x(\tau_c)\rangle(2/m_e)^{1/2}\ ,\\
P_{ca}&=i\langle\phi_s(\tau_c)\,|\,p_x\,|\,\phi_x(\tau_a)\rangle(2/m_e)^{1/2}\ ,
\end{aligned} \tag{4}$$

where $\phi_\alpha(\tau)$ denotes an atomic orbital of symmetry α, located at the position τ. τ_a and τ_c indicate the anion and cation positions in the unit cell. (m_e is the free-electron mass.) The other momentum matrix elements can be inferred by symmetry. The matrix $\langle\psi_\alpha(\mathbf{k}_t,l)\,|\,\mathbf{p}\,|\,\psi_{\alpha'}(\mathbf{k}_t,l')\rangle$ can be written in terms of P_{aa}, P_{cc}, P_{ac}, and P_{ca}.

The parameters P_{aa}, P_{cc}, P_{ac}, and P_{ca} can be directly related to the optical matrix elements associated with various interband transitions for the bulk material, which can be either measured experimentally or calculated by other reliable theoretical techniques.[18,19] The relations are provided by writing the bulk Bloch states of various bands at $\mathbf{k}=\mathbf{0}$ in terms of our tightbinding orbitals and calculating the interband transitions with these states. At $\mathbf{k}=\mathbf{0}$, the bulk Bloch states can be described in terms of the atomic orbitals as bonding and antibonding states, viz.,

$$|\,\alpha,\pm\rangle=\frac{1}{\sqrt{N}}\sum_{\mathbf{R}}[C_\alpha^{\pm}\,|\,\phi_\alpha(\mathbf{R}+\tau_a)\rangle\pm C_\alpha^{\mp}\,|\,\phi_\alpha(\mathbf{R}+\tau_c)\rangle]\ , \tag{5}$$

where $\alpha=s,\ x,\ y,\ z,\ s^*$. $\mathbf{R}$ denotes the lattice vectors and N is a normalization constant. C_α^+ and C_α^- are expansion coefficients. In this notation, the four valence-band states at $\mathbf{k}=\mathbf{0}$ are designated by $|\,s,+\,\rangle$, $|\,x,-\,\rangle$, $|\,y,-\,\rangle$, and $|\,z,-\,\rangle$, and the four lowest conduction-band states are designated by $|\,s,-\,\rangle$, $|\,x,+\,\rangle$, $|\,y,+\,\rangle$, and $|\,z,+\,\rangle$. Introducing the notations

$$\begin{aligned}
P_{++}&\equiv i\langle s,+\,|\,p_x\,|\,x,+\rangle(2/m_e)^{1/2}\ ,\\
P_{+-}&\equiv i\langle s,+\,|\,p_x\,|\,x,-\rangle(2/m_e)^{1/2}\ ,\\
P_{-+}&\equiv i\langle s,-\,|\,p_x\,|\,x,+\rangle(2/m_e)^{1/2}\ ,\\
P_{--}&\equiv i\langle s,-\,|\,p_x\,|\,x,-\rangle(2/m_e)^{1/2}\ ,
\end{aligned} \tag{6}$$

we obtain the relation

$$\begin{bmatrix}P_{aa}\\ 4P_{ac}\\ 4P_{ca}\\ P_{cc}\end{bmatrix}=\begin{bmatrix}C_x^+C_s^+ & C_x^-C_s^+ & C_x^+C_s^- & C_x^-C_s^-\\ C_x^-C_s^+ & -C_x^+C_s^+ & C_x^-C_s^- & -C_x^-C_s^+\\ C_x^+C_s^- & C_x^-C_s^- & -C_x^+C_s^+ & -C_x^+C_s^-\\ C_x^-C_s^- & -C_x^+C_s^- & -C_x^-C_s^+ & C_x^+C_s^+\end{bmatrix}\begin{bmatrix}P_{++}\\ P_{+-}\\ P_{-+}\\ P_{--}\end{bmatrix} \tag{7}$$

TABLE I. Matrix elements of V^- (in rydbergs). The notation is the same as in Ref. 19.

Material	V_1^-	V_2^-	V_3^-	V_4^-	V_5^-	V_6^-
AlAs	0.143 59	−0.108 63	0.143 71	0.164 60	−0.000 47	0.0
GaSb	0.093 15	−0.044 925	0.057 68	0.058 40	−0.105 17	0.0
InAs	0.140 90	−0.183 20	0.085 70	0.100 90	−0.232 90	0.0

In the present paper the parameters P_{++}, P_{+-}, P_{-+}, and P_{--} are extracted from the result of a full-zone $\mathbf{k}\cdot\mathbf{p}$ calculation.[18,19] The $\mathbf{k}\cdot\mathbf{p}$ parameters for GaAs are taken from Ref. 19. For AlAs we use the average $\mathbf{k}\cdot\mathbf{p}$ parameters of Si and Ge, and for GaSb and InAs we use the average of Ge and α-Sn. The matrix elements of the antisymmetric potential[19] (V^-) for these materials are adjusted to fit the experimentally measured optical gaps. The resulting matrix elements are listed in Table I. In Table II we list the parameters P_{aa}, P_{ac}, P_{ca}, and P_{cc} for GaAs, AlAs, InAs, and GaSb obtained from using Eq. (7).

B. Computation of the absorption coefficient

In a zeroth-order approximation, one may ignore the dependence of the matrix element $\mathbf{P}_{nn'}(\mathbf{k}_t,q)$ on $\mathbf{k}_t$ and q. Then Eq. (1) is simplified to

$$\alpha(\hbar\omega)=\frac{1}{\omega}\sum_{n',n}|\hat{\epsilon}\cdot\mathbf{P}_{nn'}(\mathbf{0})|^2\rho_{nn'}(\hbar\omega)\ , \tag{8}$$

where $\mathbf{P}_{nn'}(\mathbf{0})$ is the momentum matrix element evaluated at the zone center $\rho_{nn'}(\hbar\omega)$ is the joint density of states associated with the nth valence subband and the n'th conduction subband. The approximate expression (8) is commonly adopted and gives a reasonable description of the actual absorption spectrum, but it fails to explain some weak structures existing in the experimentally measured absorption spectrum.

To explain these structures, we must take into account the wave-vector dependence of the matrix elements $\mathbf{P}_{nn'}(\mathbf{k}_t,q)$. The q dependence is usually negligible for superlattices with wide barriers in which case all quantum wells are decoupled. We also take into account the nonparabolicity of the valence-band structure. The band structure for the valence subbands are far from parabolic, even for very small values of $\mathbf{k}_t$. This is due to the interaction between the closely spaced valence subbands which have different effective masses. In particular some valence subbands tend to cross each other at certain nonzero values of $\mathbf{k}_t$. Figure 1 demonstrates a typical valence-band structure of a GaAs-$Ga_{1-x}Al_xAs$ superlattice whose optical properties will be studied in detail in the next section. It is noted that the first light-hole subband (LH1) and the third heavy-hole subband (HH3) tend to cross each other at $k_t\simeq 0.012(2\pi/a)$. The second valence subband (HH2) is found to have a negative effective mass (opposite to the normal-hole mass) at the zone center and is indirect in the sense it has a maximum at a nonzero value of k_t. Furthermore, it tends to cross the first subband (HH1), thus giving rise to a dip in the HH1 subband at $k_t\simeq 0.008(2\pi/a)$.

To simplify the computation, we assume that both the band structure and the matrix element $\mathbf{P}_{nn'}(\mathbf{k}_t,q)$ depend only on the absolute value of $\mathbf{k}_t$ (i.e., we ignore the anisotropy in the $\mathbf{x}$-$\mathbf{y}$ plane). This is found to be a good approximation as can be seen from Fig. 1. With this approximation the summation over $\mathbf{k}_t$ in (1) can be replaced by a one-dimensional integral over k_t. For thick superlattices, we ignore the q dependence. The squared optical matrix element and energy values are computed at 10—20 sampling $\mathbf{k}_t$ points along a given direction ([100] or [110]) over the range of interest. These values on a much finer mesh (about 200 points) are then interpolated by cubic splines. Finally the integral over k_t in (1) is performed numerically. For thin superlattices, we assume that the subband energy (E_n) and the squared optical matrix element ($Q_{nn'}$) can be approximated by the expressions

$$E_n(\mathbf{k}_t,q)=E_n(\mathbf{k}_t,0)+E_n(0,q)-E_n(0,0) \tag{9a}$$

and

$$Q_{nn'}(\mathbf{k}_t,q)=Q_{nn'}(\mathbf{k}_t,0)Q_{nn'}(0,q)/Q_{nn'}(0,0)\ , \tag{9b}$$

where

$$Q_{nn'}(\mathbf{k}_t,q)\equiv\frac{2}{m_e}|\hat{\epsilon}\cdot\mathbf{P}_{nn'}(\mathbf{k}_t,q)|^2\ .$$

The expression (9a) is appropriate for E_n because it reduces to the effective-mass approximation in the limit of small $\mathbf{k}_t$ and q. The expression 9(b) is appropriate for $Q_{nn'}$ because it ensures positive values of $Q_{nn'}$ at any $\mathbf{k}_t$ and q. For small values of $\mathbf{k}_t$ and q, the expressions 9(a) and 9(b) are nearly equivalent. The functions $E_n(\mathbf{0},q)$ and $Q_{nn'}(\mathbf{0},q)$ are also calculated on about ten sampling q

TABLE II. Optical matrix elements between tight-binding orbitals. The unit is $(eV)^{1/2}$.

Material	P_{aa}	P_{ac}	P_{ca}	P_{cc}
GaAs	2.860	0.265	−0.960	2.485
AlAs	2.896	0.081	−0.868	1.876
InAs	2.403	0.116	−0.866	2.349
GaSb	3.006	0.115	−0.804	1.992

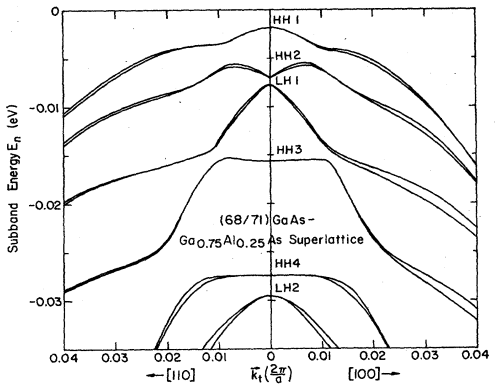

FIG. 1. Valence-subband energies of the (68/71) GaAs-$Ga_{0.75}Al_{0.25}As$(001) superlattice plotted as functions of the parallel wave vector ($\mathbf{k}_t$) along the [100] and [110] directions.

points along the [001] direction, and then interpolated by cubic splines. The two-dimensional integral over $\mathbf{k}_t$ and q in (1) is then performed numerically.

C. Symmetry properties and selection rules

In order to analyze the optical properties of the superlattice, it is essential to understand the symmetry properties of the electronic states involved. Because of the inclusion of the spin-orbit interaction in our tight-binding model, it is more convenient to describe the superlattice electronic states in terms of a set of atomic basis states which are eigenstates of the total angular momentum (the vector addition of the spin and the atomic orbital angular momentum). This set of basis states are linear combinations of the products of the atomic orbitals, ϕ_α, and the spinors (denoted by $\uparrow$ or $\downarrow$). They are given by

$$\begin{aligned}
&\omega_{\mathrm{C}}=\phi_s^{\downarrow}\ ,\\
&\omega_{\mathrm{C}^*}=\phi_{s^*}^{\downarrow}\ ,\\
&\omega_{\mathrm{HH}}=-(\phi_x^{\uparrow}+i\phi_y^{\uparrow})/\sqrt{2}\ ,\\
&\omega_{\mathrm{LH}}=(\phi_x^{\uparrow}-i\phi_y^{\uparrow}+2\phi_z^{\downarrow})/\sqrt{6}\ ,\\
&\omega_{\mathrm{SO}}=(\phi_x^{\uparrow}-i\phi_y^{\uparrow}-\phi_z^{\downarrow})/\sqrt{3}
\end{aligned} \tag{10}$$

and their charge conjugates: $\bar{\omega}_{\mathrm{C}}$, $\bar{\omega}_{\mathrm{C}^*}$, $\bar{\omega}_{\mathrm{HH}}$, $\bar{\omega}_{\mathrm{LH}}$, and $\bar{\omega}_{\mathrm{SO}}$. The charge conjugates $\bar{\omega}_j$ ($j=$C, C*, HH, LH, SO) are related to ω_j by flipping the spin and changing ϕ_x to $-\phi_x$. At the zone center, the bulk conduction, heavy-hole, light-hole, and split-off (SO) states are just the antibonding and bonding states made up of the ω_{C}, ω_{HH}, ω_{LO}, and ω_{SO} atomic orbitals associated with the anion and cation. For the superlattice, if we consider the case $\mathbf{k}_t=\mathbf{0}$, then the two sets of $\{\omega_j\}$ and $\{\bar{\omega}_j\}$ are decoupled and all the superlattice energy levels are doubly degenerate. Let us consider the symmetry property of the bulk tight-binding Hamiltonian (H) written in the basis set $\{\omega_j\}$. For $\mathbf{k}_t=\mathbf{0}$, one can show that H is invariant under the transformation: $\omega_{\mathrm{C}}\rightarrow\omega_{\mathrm{C}}$, $\omega_{\mathrm{C}^*}\rightarrow\omega_{\mathrm{C}^*}$, $\omega_{\mathrm{HH}}\rightarrow\omega_{\mathrm{HH}}$, $\omega_{\mathrm{LH}}\rightarrow-\omega_{\mathrm{LH}}$, $\omega_{\mathrm{SO}}\rightarrow-\omega_{\mathrm{SO}}$, and $k_z\rightarrow-k_z$, where z is the direction perpendicular to the interface. The above symmetry property implies that the light-hole and split-off components are odd and the conduction (C) and heavy-hole (HH) components are even under the reflection with respect to the x-y plane. Similar to Eq. (2), the superlattice electronic states $|\,n,\mathbf{k}_t,q\,\rangle$ can be expanded in terms of a new set of planar atomic orbitals $\psi_j(\mathbf{k}_t,l)$ which are related to the old planar orbitals $\psi_\alpha(\mathbf{k}_t,l)$ by the transformation given in Eq. (10). Thus

$$|\,n,\mathbf{k}_t,q\,\rangle=\sum_{j,l}A_j^n(\mathbf{k}_t,q,l)\,|\,\psi_j(\mathbf{k}_t,l)\,\rangle\ . \tag{11}$$

Here $j=$C,C*, HH, LH, SO, and their charge conjugates. The $A_j(l)$ (omitting the label $\mathbf{k}_t,q$) shall be referred to as the j-component envelope function. When the superlattice is dominated by only one j component, the associated envelope function $A_j(l)$ may be obtained to a good approximation by the envelope-function method (EFM) and the symmetry of $A_j(l)$ is determined by the principal quantum number n. For example, for the highest valence subband state (VB1), the heavy-hole component dominates and $n=1$. Thus $A_{\mathrm{HH}}^{\mathrm{VB1}}(l)$ and $A_{\mathrm{C}}^{\mathrm{VB1}}(l)$ are even, whereas $A_{\mathrm{LH}}^{\mathrm{VB1}}(l)$ and $A_{\mathrm{SO}}^{\mathrm{VB1}}(l)$ are odd under the transformation $l\rightarrow-l$ ($l=0$ at the center of the well). It is interesting to note that in any superlattice state the HH and C-component envelope functions of a given parity are always mixed with the LH and SO-component envelope functions of the opposite parity. As described in I, the valence-subband states identified as the $n=2$ heavy-hole (HH2) state and the $n=1$ light-hole (LH1) state can couple to each other strongly, when their energies become close to each other at certain well width. This coupling can lead to a crossover phenomenon in the optical transitions as will be demonstrated in the next section.

For $\mathbf{k}_t\neq\mathbf{0}$, the situation is somewhat more complicated. In this case, the two sets $\{\omega_j\}$ and $\{\bar{\omega}_j\}$ are coupled together and every superlattice state contains all ten components. To analyze the symmetry property of the envelope function associated with each component, we consider the bulk Luttinger-Kohn Hamiltonian[20] [$H_0(\mathbf{k})$] for describing the hole near the zone center (assuming infinite spin-orbit splitting)

$$H_0(\mathbf{k})=\begin{bmatrix} P+Q & L & M & 0\\ L^* & P-Q & 0 & M\\ M^* & 0 & P-Q & L\\ 0 & M^* & L^* & P+Q \end{bmatrix}, \tag{12}$$

where

$$\begin{aligned}
&P=\gamma_1 k^2\ ,\\
&Q=\gamma_2(k_x^2+k_y^2-2k_z^2)\ ,\\
&L=-2\sqrt{3}\gamma_3(k_x-ik_y)k_z\ ,\\
&M=-\sqrt{3}\gamma_2(k_x^2-k_y^2)+i2\sqrt{3}\gamma_3 k_x k_y\ ,
\end{aligned}$$

and γ_1, γ_2, and γ_3 are the Luttinger parameters. The basis states for the above 4×4 matrix are ω_{HH}, ω_{LH}, $\bar{\omega}_{\mathrm{LH}}$, and $\bar{\omega}_{\mathrm{HH}}$. To adapt this Hamiltonian to the (001) superlattice, we replace the z component of the wave vector k_z by the operator $(P_z/\hbar)$ which operates on the envelope

functions. The parallel components of the wave vector k_x and k_y remain good quantum numbers. For a fixed value of $\mathbf{k}_t=(k_x,k_y)$, we see that ω_{HH} is coupled with ω_{LH} by a term (L) proportional to P_z, and with $\bar{\omega}_{LH}$ by a term (M) independent of P_z. Because P_z is odd under the reflection with respect to the x-y plane, an even HH-component envelope function will be coupled with an odd LH-component and an even $\overline{LH}$-component envelope function, and vice versa. A similar argument applies to the coupling of $\bar{\omega}_{HH}$ with $\bar{\omega}_{LH}$ and ω_{LH}. The two sets of envelope functions (even HH, odd LH, even $\overline{LH}$, odd $\overline{HH}$) and (odd HH, even LH, odd $\overline{LH}$, even $\overline{HH}$) are decoupled as far as H_0 is concerned. In the envelope-function approximation, one assumes that the superlattice potential is diagonal in the basis used; thus all energy levels are doubly degenerate.

The above discussion may cause some confusion, since in the bulk semiconductor, there exists no degeneracy at a general $\mathbf{k}$ point (both $\mathbf{k}_t\neq\mathbf{0}$ and $k_z\neq0$). However, because the bulk Hamiltonian is invariant under time reversal and the operation ($x\rightarrow-x$ and $y\rightarrow-y$), we have $E(\mathbf{k}_t,k_z)=E(\mathbf{k}_t,-k_z)$, and the Bloch states $\psi(\mathbf{k}_t,k_z)$ and $\psi(\mathbf{k}_t,-k_z)$ are related by the charge conjugation and the operation ($z\rightarrow-z$). The superlattice potential mixes two pairs of spin-split heavy-hole states and two pairs of light-hole states at k_z and $-k_z$ together. If the potential is diagonal in the basis (HH, LH, $\overline{LH}$, $\overline{HH}$), then the diagonalization will result in four pairs of doubly degenerate superlattice states. In the tight-binding model, the potential contains off-diagonal terms which will split the degeneracy and couple even and odd envelope functions associated with all components together. This leads to asymmetry envelope functions for all components in the superlattice valence subband states when $\mathbf{k}_t\neq\mathbf{0}$. This kind of result is not obtainable from the envelope-function approach.

The selection rules for optical transitions in superlattices are intimately related to the symmetry properties discussed above. It is generally accepted that based on the envelope-function analysis, the optical transitions in superlattices must satisfy the selection rule $\Delta n=0$. This is because the overlap of envelope functions associated with the conduction and valence subbands vanishes when $\Delta n\neq0$. This selection rule is invalidated when states associated with different n (defined in EFM) are coupled together in a given superlattice state. This is found to be the case for the optical transitions involving the second and third valence subbands, because of the mixing of LH1 and HH2 states mentioned above. Besides this special case (which only occurs for superlattices of some particular well widths), the $\Delta n=0$ selection rule is also not valid when we consider the $\mathbf{k}_t\neq\mathbf{0}$ case. This is due to the coupling of HH and LH envelope functions of both parities at $\mathbf{k}_t\neq\mathbf{0}$. Thus some weak structures will become present in the absorption spectrum near the energy region which is forbidden according to the $\Delta n=0$ selection rule.

The selection rules for different polarization of the incident light can also be established. Since the conduction-subband states are almost purely s like, for light polarized along the z direction only transitions associated with the LH and SO components are possible, whereas for light polarized along the $[x,y]$ direction, transitions associated with the HH, LH, and SO components are all possible. For the (x,y)-polarized case, the oscillator strength of the HH component is three times that of the LH component since

$$|\langle\omega_C|p_x|\omega_{HH}\rangle|^2=3|\langle\omega_C|p_x|\omega_{LH}\rangle|^2 .$$

[See Eq. (10).]

III. RESULTS AND DISCUSSIONS

A. GaAs-$Ga_{1-x}Al_xAs$ superlattices

We shall first discuss the behavior of the squared optical matrix elements $Q_{nn'}(\mathbf{k}_t,q)$, and then the absorption coefficients. In Fig. 2 the squared optical matrix elements at zone center, $Q_{nn'}(\mathbf{0},0)$, for transitions from the highest three valence subbands (labeled VB1-VB3) to the two lowest conduction subbands (labeled CB1 and CB2) for GaAs-$Ga_{0.7}Al_{0.3}As$ superlattices with 20 alloy layers ($M=20$) are plotted as functions of the number of GaAs layers (N). The corresponding energy levels for the valence subbands as functions of N have been shown in Fig. 6 of I. The strength of the optical matrix element depends on the polarization of the incident light, $\hat{\mathbf{e}}$. In Fig. 2, (z) denotes the component perpendicular to the interface, and (x,y) denotes the sum of the x and y components [i.e., $(2/m_e)(|\hat{\mathbf{x}}\cdot\mathbf{P}_{nn'}|^2+|\hat{\mathbf{y}}\cdot\mathbf{P}_{nn'}|^2)$]. For unpolarized light propagating perpendicular to the interface (the normal experimental condition), the squared optical matrix elements are one-half of those shown by the curves labeled with (x,y). The matrix element for the VB1-CB1 transition has the (x,y) component only and is almost independent of the GaAs well width. The matrix elements for the VB2-CB1 and VB3-CB1 transitions cross each other at $N\simeq68$. The behavior of the matrix elements as functions of N can be understood by examining the superlattice wave functions of the valence-band states (VB1-VB3). As described in I, the VB1 state is dominated by the heavy-hole bulk state for any N, whereas the VB2 and VB3 states contain admixtures of heavy- and light-hole

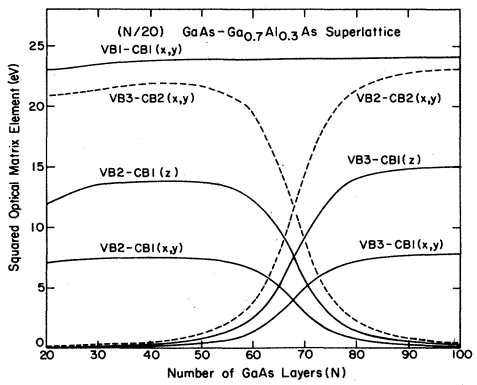

FIG. 2. Squared optical matrix elements for GaAs-$Ga_{0.7}Al_{0.3}As$ superlattices with 20 alloy layers plotted as functions of the number of GaAs layers (N).

bulk states which vary with N. At N much less than N_c (the layer thickness at which the crossing occurs) the VB2 and VB3 states can be identified as the first light-hole (LH1) and the second heavy-hole (HH2) states, respectively. At N much greater than N_c, the two states switch roles. At N near N_c, the two states have comparable admixtures of the heavy-hole and light-hole bulk states. Since the overlap between the envelope functions of the HH2 and CB1 states vanishes, the magnitude of the matrix element is determined by the amount of LH1 character in the two valence-band states. Therefore, the ratio of the x component to the z component in the squared optical matrix element is approximately 1:4 [see Eq. (10)]. Furthermore, a crossing behavior in the optical matrix element occurs due to the varying strength of LH1 components in the two valence-band states.

As shown in Fig. 2, the mixing of LH1 and HH2 states also leads to a crossing behavior in the optical matrix elements for the transitions from the VB2 and VB3 states to the CB2 state. In this case the magnitude of the matrix element is determined by the amount of HH2 component in the valence-subband states. Hence, the z-component matrix element vanishes.

The aforementioned HH2-LH1 crossing effect should be found in all GaAs-$Ga_{1-x}Al_xAs$ superlattices, but the value of N_c will depend on the composition x and the number of layers of the barrier material (M). The value of N_c as a function of M for various alloy compositions of the barrier material has been illustrated in Fig. 9 of I.

Next, we discuss the dependence of squared optical matrix elements $Q_{nn'}(\mathbf{k}_t,0)$ on the parallel wave vector, $\mathbf{k}_t$. We consider a GaAs-$Ga_{0.75}Al_{0.25}As$ (001) superlattice with 68 GaAs layers (190 Å) and 71 alloy layers (200 Å). The valence-band structures along the [100] and [110] directions have been shown in Fig. 1. The (x,y) and z component squared optical matrix elements as functions of $\mathbf{k}_t$ for transitions from the top four valence subbands to the first conduction subbands are shown in Figs. 3 and 4, respectively. In each transition, two nearly degenerate

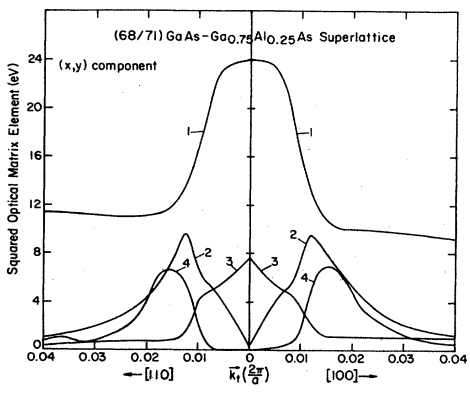

FIG. 3. (x,y) component squared optical matrix elements for the (68/71) GaAs-$Ga_{0.75}Al_{0.25}As$(001) superlattice plotted as functions of the parallel wave vector ($\mathbf{k}_t$) along the [100] and [110] directions.

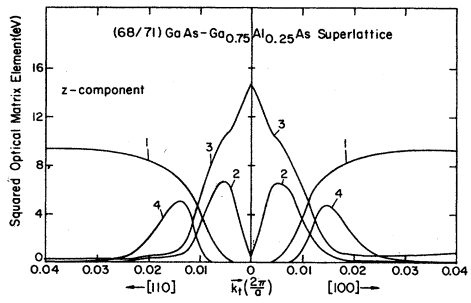

FIG. 4. z-component squared optical matrix elements for the (68/71) GaAs-$Ga_{0.75}$-$Al_{0.25}As$(001) superlattice plotted as functions of the parallel wave vector ($\mathbf{k}_t$) along the [100] and [110] directions.

valence and conduction subbands are involved. For each squared optical matrix element we have summed over the two final conduction states and averaged over the two initial valence states. We found dramatic changes in the optical matrix elements as k_t is varied over a small range (one-twentieth of the Brillouin zone). This is due to the strong mixing between various HH and LH components by the off-diagonal terms of H_0 given in (12). The variation of the optical matrix elements can also be understood qualitatively by considering the mixing of various valence subbands at $\mathbf{k}_t \neq 0$. From Fig. 1, we see that HH1 and HH2 interact strongly at $k_t \simeq 0.01(2\pi/a)$. This leads to a large reduction in the HH1-CB1 transition and a compensating enhancement in the HH2-CB1 transition near $k_t = 0.01(2\pi/a)$ (see Fig. 3). Similarly, the mixing of LH1 and HH3 at $k_t \simeq 0.01(2\pi/a)$ gives rise to the crossover behavior in the optical matrix elements of the LH1-CB1 and HH3-CB1 transitions. Analogous effects are also seen in Fig. 4. It is noted from Figs. 3 and 4 that all pairs of optical transitions are dipole allowed at $\mathbf{k}_t \neq 0$ This finding is different from what one would expect from a simple envelope-function approach which considers one conduction and one valence band only.[10] To give more insight into the band-mixing phenomena at $\mathbf{k}_t \neq 0$, we show in Fig. 5 the valence-subband wave functions of VB1 and VB2 at $\mathbf{k}_t = (0.01,0)(2\pi/a)$ as well as those of VB3 and VB4 at $\mathbf{k}_t = (0.012,0)(2\pi/a)$, where the strongest band mixing occurs. We have plotted the sum of the squared anion and cation coefficients associated with the HH (solid), $\overline{HH}$ (dotted), LH (dashed), and $\overline{LH}$ (dotted-dashed) components. Since each subband is nearly doubly degenerate, the wave function of the two states of each pair are nearly identical with the ω_j components replaced by $\bar{\omega}_j$. Thus only one state per subband is shown. The j-component squared amplitude at a layer l is defined as $|A_j^n(\mathbf{k}_t q,l)|^2$ summed over the anion and cation contributions. As shown in this figure, all four wave functions have strong admixtures of heavy- and light-hole components. Furthermore, the envelope functions no longer have well-defined parity.

Finally, we discuss the absorption spectrum calculated by the method described in Sec. II B. Figure 6 shows the absorption coefficients for separate transitions between the top six valence subbands (VB1-VB6) and the bottom

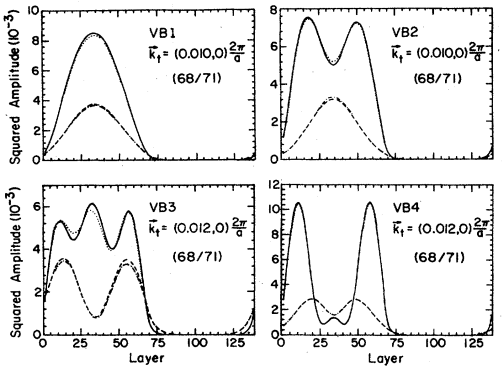

FIG. 5. Squared amplitudes associated with the HH (solid), $\overline{HH}$ (dotted), LH (dashed), and $\overline{LH}$ (dashed-dotted) components of various valence-band states at certain nonzero values of $\mathbf{k}_t$ for the (68/71) GaAs-$Ga_{0.75}Al_{0.25}As$ superlattice.

two conduction subbands (CB1 and CB2), each subband being nearly doubly degenerate. Figure 7 shows the total absorption coefficient from VB1-VB6 to CB1-CB3. We assume that the incident light is propagating perpendicular to the interface; thus only the (x,y) component is considered. It is found that the overall shape of the absorption coefficient is close to the staircase function as predicted by the simple approximation described by (8), although each step tends to decline somewhat toward the high-energy side. The decline is faster than the $1/\omega$ factor introduced in (1) and is due to the decrease of momentum matrix element with increasing k_t, as can be seen in Fig. 3. Note that the absorption coefficient in Figs. 6 and 7 is truncated at $\hbar\omega \simeq 1.6$ eV, above which the VB1 states

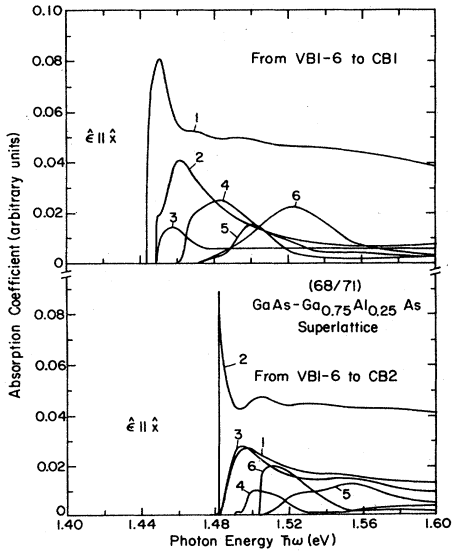

FIG. 6. Absorption coefficient corresponding to separate optical transitions from the VB1-VB6 to CB1 (top panel) and to CB2 (bottom panel) for the (68/71) GaAs-$Ga_{0.75}Al_{0.25}As$ superlattice.

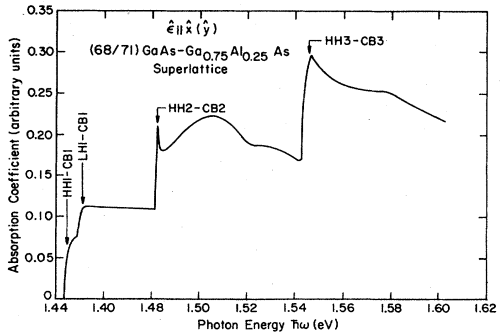

FIG. 7. Absorption coefficient of the (68/71) GaAs-$Ga_{0.75}Al_{0.25}As$ superlattice.

with $k_t > 0.04(2\pi/a)$ begin to contribute and the spherical approximation used will gradually become invalid (see Fig. 1).

Despite the strong variation of the squared matrix elements for various pairs of optical transitions, the net absorption spectrum remains nearly structureless, except for a small sharp peak marked HH2-CB2. This is not surprising, since the sum of oscillator strengths for optical transitions from any two interacting valence states to a given conduction state must remain constant despite the mixing. However, when the exciton effect is also taken into account, we expect that the inclusion of band mixing will lead to nonzero oscillator strength for some excitons which are otherwise optically inactive. The sharp peak marked HH2-CB2 deserves some mention. This sharp peak arises from the negative effective mass of the HH2 subband at the zone center (see Fig. 1). If the effective mass of this subband can be adjusted by changing the GaAs well width and the barrier-alloy concentration such that it equals the negative of the electron effective mass, then a singularity in the joint density of states results, and a δ-function—type structure would occur in the absorption spectrum. Sanders and Chang[21] have made a systematic study of such a phenomenon in modulation-doped semiconductor quantum wells using a multiband effective-mass approach which is also capable of including the heavy- and light-hole mixing at $\mathbf{k}_t \neq 0$. They found that such a strong sharp peak can indeed be created if one chooses a GaAs well width of ~ 100 Å and a barrier-alloy composition (x) of ~ 0.4.

To facilitate comparison with the experimental data, we need to include the exciton effect as well. Since the paper puts emphasis on the band-to-band transition, we shall use a very simple model to describe the exciton effect. We assume that (i) the binding energy of the two-dimensional exciton is about 7 meV (Ref. 22) for all pairs of transitions. (ii) The absorption for each exciton is described by a Lorentzian function $(f_0\Gamma/\pi)/[(E-E_0)^2+\Gamma^2]$ with half width Γ which is adjusted to mimic the experimental structure, and (iii) the oscillator strength (f_0) of each exciton peak is given by

$$f_0 = \left| \sum_{k_t} \Phi_{ex}(\mathbf{k}_t)\hat{\epsilon}\cdot\mathbf{P}_{nn'}(\mathbf{k}_t,0) \right|^2 ,$$

where $\Phi_{ex}(\mathbf{k}_t)$ is the exciton envelope function in $\mathbf{k}_t$ space. In the spherical approximation, the two-dimensional exciton has an envelope function

$$\Phi_{ex}(\rho)=\left[\frac{2}{\pi}\right]^{1/2}\frac{1}{a_0}e^{-\rho/a_0}[\rho\equiv(x^2+y^2)^{1/2}]$$

and a binding energy $E_x=(e^2/\epsilon_0 a_0)$, where a_0 is the radius of the exciton. Thus for $E_x=7$ meV, $a_0\simeq 144$ Å and

$$\Phi_{ex}(\mathbf{k}_t)=\frac{\sqrt{8\pi}}{a_0^2}(k_t^2+1/a_0^2)^{-3/2}\ .$$

Given the interband optical matrix element $\hat{\epsilon}\cdot\mathbf{P}_{nn'}(\mathbf{k}_t,0)$ as a function of k_t, the oscillator strength f_0 can be evaluated.

The result of including the exciton effect and the corresponding experimental data obtained from Ref. 13 are shown in Fig. 8. The entire spectrum is scaled such that the integrated strength (f_0) of the HH2-CB2 exciton agrees with the data. The broadening widths (Γ) which fit the six prominent exciton peaks are 1,1, 2,2, 4, and 6 meV. The band-to-band transition has also been broadened by a Lorentzian function with a half width $\Gamma=2$ meV and scaled to match the experimental data. The agreement between theory and experiment is fairly good. The previously unexplained structure indicated by a question mark is now accounted for by the hump resulting from the HH3-CB1 transition. This transition is no longer forbidden when we take into account the $\mathbf{k}_t\neq\mathbf{0}$ contributions. As shown in Fig. 3, the squared optical matrix element for the HH3-CB1 transition (labeled by 4) increases with k_t and reaches a value of about 20% of the zone-center HH1-CB1 transition at $k_t=0.017(2\pi/a)$.

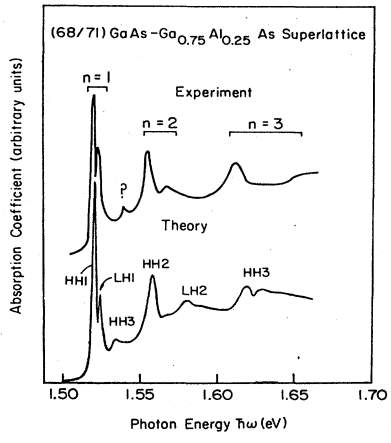

FIG. 8. Theoretical and experimental absorption coefficient of the (68/71) GaAs-$Ga_{0.75}Al_{0.25}As$ superlattice, including the exciton effect. The experimental spectrum was taken by R. Dingle (Ref. 13). The theoretical spectrum has been rigidly shifted in energy for direct comparison.

This is a result of the band-mixing effect discussed in Sec. II C. There is, however, a discrepancy between the theory and experiment: The theoretically predicted energy of this hump is about 5 meV too low. This could be due to the fact that the hole effective masses used here are different from the "true" effective masses. The heavy-hole effective mass used here is $0.45m_e$.[23] However, the value deduced from the $\mathbf{k}\cdot\mathbf{p}$ theory by Lawaetz[24] is $0.35m_e$. If the latter value is used, then the energy of this hump will agree with the experimental data to within 1 meV. Note that the exciton binding energy used here should also have an uncertainty of at least 1 meV.

B. InAs-GaSb superlattices

InAs-GaSb superlattices differ from GaAs-$Ga_{1-x}Al_xAs$ superlattices in that the electron and hole are confined in different materials. The spatial separation of the electron and hole substantially suppresses the strength of possible optical transitions between conduction- and valence-subband states. Thus interesting optical properties are found only in superlattices of small well width. The squared optical matrix elements at zone center $Q_{nn'}(0,0)$ for transitions from the highest three valence subbands (labeled VB1-VB3) to the lowest two conduction subbands (labeled CB1 and CB2) for InAs-GaSb superlattices with 10 InAs layers ($M=10$) are plotted as functions of the number of GaSb layers (N) in Fig. 9. The corresponding valence subband energies as functions of N have been shown in Fig. 14 of I.

We find that the squared optical matrix element for the VB1-CB1 (or HH1-CB1) transition decreases monotonically with increasing N. In the units used here, the bulk InAs and GaSb optical matrix elements squared $[(2/m_e)|\langle s|P_x|x\rangle|^2]$ are 20.9 and 20.1 eV, respectively. The squared optical matrix elements for VB2-CB1 and VB3-CB1 cross each other at $N\simeq 15$ due to the LH1-HH2 mixing effect. The sum of $Q_{nn'}$ for all polarizations associated with these two transitions is equal to the LH1-CB1 oscillator strength in the absence of the LH1-HH2

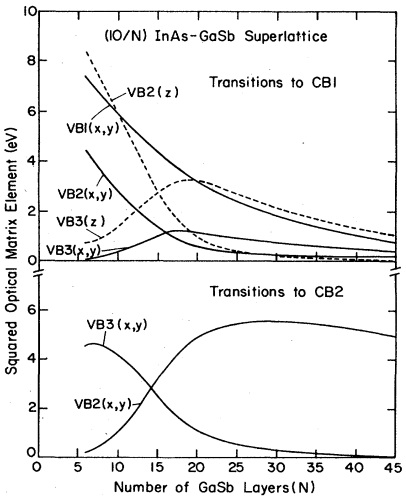

FIG. 9. Squared optical matrix elements for InAs-GaSb superlattices with 10 InAs layers plotted as functions of the number of GaSb layers (N).

mixing. This unmixed LH1-CB1 oscillator strength decreases monotonically with increasing N and is found to be nearly twice as large as the HH1-CB1 oscillator strength for all N. In comparison, for the GaAs-$Ga_{1-x}Al_xAs$ superlattice, the HH1-CB1 and the unmixed LH1-CB1 oscillator strengths are nearly identical for all N (see Fig. 2).

We can understand the behavior of the optical matrix elements described above qualitatively by analyzing the superlattice wave functions. Because of the spatial separation of the conduction- and valence-band states, the magnitude of the optical matrix element is essentially determined by the decay lengths in the barrier material (InAs for the valence-band states or GaSb for the conduction-band states) in the initial and final states. In the envelope-function approximation, the $(n=1)$ optical matrix element is proportional to the overlap integral given by

$$\frac{1}{\sqrt{S_1 S_2}}\left[\int_0^{Na'} e^{-z/\lambda_1}\cos(k_2 z)dz + \int_0^{Ma'} e^{-z/\lambda_2}\cos(k_1 z)dz\right], \tag{13}$$

where S_1, S_2 are the normalization constants, which are approximately proportional to M and N. λ_1, λ_2 are the decay lengths and k_1, k_2 are the allowed wave numbers associated with the conduction and valence states. a' is the layer thickness ($a'=3.05$ Å). Hence, for sufficiently large $N(\gtrsim 10)$, the first integral inside the large parentheses of (13) is nearly constant and the oscillator strength goes approximately as $1/N$. We define the decay length as the inverse of the imaginary part of the complex wave vector associated with the energy of the superlattice state. The complex band structures of InAs and GaSb have been shown in Fig. 10 of I. For N between 5 and 45 the conduction-state decay length (λ_1) is between $6a'$ and $9a'$; the valence-band decay length (λ_2) for the HH component is between $1.5a'$ and $1.7a'$ and that for the LH component is between $13a'$ and infinity (see Figs. 10 and 14 of I). Thus, for the HH1-CB1 transition, the first term in (13) dominates, and for the LH1-CB1 transition both terms in (13) contribute. This consideration leads to a larger oscillator strength for the unmixed LH1-CB1 transition than for the HH1-CB1 transition. The valence-band structures along the [100] and [110] directions for a (10/10) InAs-GaSb superlattice are plotted in Fig. 10. Because of the strong spin-orbit interaction and the large perturbation introduced at the interfaces, each valence subband has a sizable splitting at $\mathbf{k}_t \neq \mathbf{0}$. We label the higher spin-split states in the top three valence subbands by 1-3 and the lower spin-split states by 1′-3′. We note that the conduction subbands also have a small splitting at $\mathbf{k}_t \neq \mathbf{0}$, which we shall ignore. The squared optical matrix elements $Q_{nn'}(\mathbf{k}_t, 0)$ for transitions from the top three pairs of valence subbands (VB1-VB3) to the first pair of conduction subbands (CB1) as functions of $\mathbf{k}_t$ for a (10/10) InAs-GaSb superlattice are plotted in Fig. 11 [$\hat{\epsilon}||\hat{x}(\hat{y})$] and Fig. 12 ($\hat{\epsilon}||\hat{z}$). We have summed over the contributions to the two final conduction states, since they are nearly degenerate. As shown in Fig. 11 [$\hat{\epsilon}||\hat{x}(\hat{y})$], the squared optical matrix elements of VB1-CB1 and VB2-CB1 transitions decrease rapidly whereas the VB3-CB1 transition increases slowly as k_t increases. In Fig. 12 ($\hat{\epsilon}||\hat{z}$), the VB2-CB1 transition decays rapidly, whereas the VB1-CB1 and VB3-CB1 transitions grow in a compensating way. The sum of the squared optical matrix

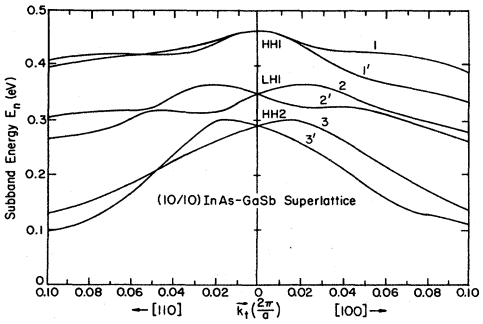

FIG. 10. Valence-subband energies of the (10/10) InAs-GaSb(001) superlattice plotted as functions of the parallel wave vector ($\mathbf{k}_t$) along the [100] and [110] directions.

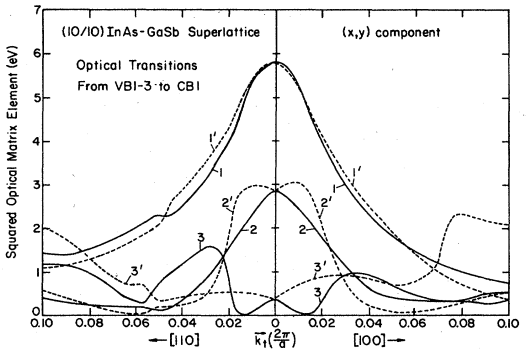

FIG. 11. (x,y) component squared optical matrix elements for the (10/10) InAs-GaSb (001) superlattice plotted as functions of the parallel wave vector ($\mathbf{k}_t$) along the [100] and [110] directions.

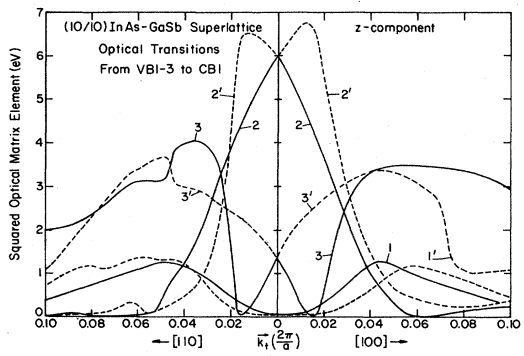

FIG. 12. z-component squared optical matrix elements for the (10/10) InAs-GaSb(001) superlattice plotted as functions of the parallel wave vector ($\mathbf{k}_t$) along the [100] and [110] directions.

elements of these transitions (VB1-VB3 to CB1) is nearly constant for $\hat{\mathbf{e}}||\hat{\mathbf{z}}$, but is a decaying function of k_t for $\hat{\mathbf{e}}||\hat{\mathbf{x}}(\hat{\mathbf{y}})$. This can be understood as follows. The increase of k_t causes a decrease in the conduction-band decay length (λ_1): λ_1 varies from $6a'$ to $4a'$ for k_t from 0 to $0.05(2\pi/a)$. As a consequence, the CB1 wave function becomes more and more confined when k_t increases. Since the HH component envelope function is always much more confined than the conduction-envelope function, the increasing confinement of the latter leads to a decreasing oscillator strength for transitions involving heavy-hole states. Thus the (x,y) component decreases with k_t.

Because the superlattice considered here is thin, the q dependence of the subband energies and optical matrix elements cannot be ignored. Figure 13 shows the subband energies (E_n) and squared optical matrix elements ($Q_{nn'}$) as functions of the perpendicular wave vectors (q) A rather large dispersion is found in all subbands except the VB1. The VB1 is nearly dispersionless, because the HH decay length is very short ($\lambda \simeq 1.5a'$). The effective mass for CB1 along the [001] direction is found to be $\sim 0.037 m_e$. A HH2-LH1 crossing is found to occur at $q \simeq 0.02(2\pi/a)$ for the VB2 and VB3 subbands. This leads to a crossover behavior in the $Q_{nn'}$ of VB2 and VB3 as functions of q. The total oscillator strength for the VB1-VB3 to CB1 transitions decreases rather quickly as q goes from Γ to X, while a compensating increase is found in the total oscillator strength for the VB1-VB3 to CB2 transitions (not shown). This can be understood in terms of the band mixing between CB1 and CB2.

The absorption coefficient for this superlattice is calculated according to the procedures described in Sec. II B. The result is shown in Fig. 14. The absorption spectrum is found to be nearly structureless, although various interband transitions can still be identified as shoulder structures. This is in qualitative agreement with the experimental data.[10] The structureless absorption is due to the fact that the thin superlattice considered here has strong dispersion in the conduction-band structure along all directions. Thus the resulting absorption spectrum is like that of a three-dimensional bulk material.

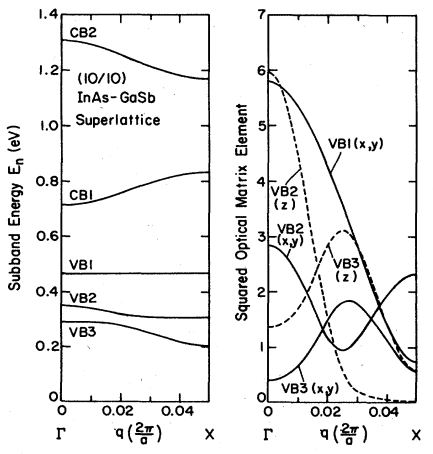

FIG. 13. Subband energies and squared optical matrix elements for the (10/10) InAs-GaSb(001) superlattice plotted as functions of the perpendicular wave vector (q).

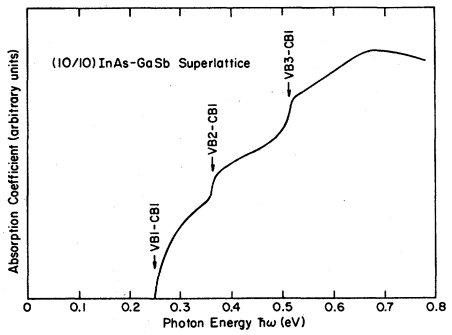

FIG. 14. Absorption coefficient of the (10/10) InAs-GaSb superlattice.

IV. CONCLUDING REMARKS

We have studied the optical properties of GaAs-$Ga_{1-x}Al_xAs$ and InAs-GaSb superlattices. The subband energies and squared optical matrix elements are calculated as functions of well thickness (N), parallel wave vector ($\mathbf{k}_t$), and perpendicular wave vector (q). We find that the band-mixing effect causes the valence-subband energies and the optical matrix elements to vary nontrivially with N, $\mathbf{k}_t$, and q. This effect can sometimes lead to unexpected features in the photoabsorption spectrum. In particular we show that the weak structure corresponding to the forbidden HH3-CB1 transition can now be explained in terms of the band mixing and the exciton effect.

For InAs-GaSb superlattices, we show that the oscillator strength for various optical transitions decreases with the GaSb thickness (N) approximately like $1/N$. If the InAs thickness (M) is also varied, it can be deduced that the oscillator strength decreases like $1/MN$. Thus detectable optical signals can only be obtained for thin superlattices. We find that the photoabsorption spectrum of the thin InAs-GaSb superlattice is nearly structureless, similar to what one expected from a three-dimensional bulk material. However, it is possible to obtain a two-dimensional absorption spectrum by making a superlattice with thick GaSb (e.g., 40 layers) and thin InAs (e.g., 10 layers). The InAs does not have to be thick, because the heavy-hole decay length is extremely short. The oscillator strength for such a superlattice is about six times lower than the (10/10) superlattice (see Fig. 9) and may still be detectable. With the modulation doping, it is possible to create confining triangular potentials for both the electron and the hole on the two sides of a given interface. thus the oscillator strength for interband transitions could be enhanced due to the increasing overlap between the electron and hole envelope functions in modulation-doped InAs-GaSb superlattices.

ACKNOWLEDGMENTS

We gratefully acknowledge fruitful discussions with G. Osbourn and G. D. Sanders. We also acknowledge the use of the computing facility provided by the University of Illinois Materials Research Laboratories under the National Science Foundation grant. This work was supported by the U. S. Office of Naval Research under Contracts Nos. N00014-81-K-0430 and N00014-82-K-0458.

---

*Present address: Hughes Research Laboratories, 3011 Malibu Canyon Road, Malibu, CA 90265.

[1]For a review, see, for example, L. L. Chang and L. Esaki, in *Progress in Crystal Growth and Characterization,* edited by B. R. Pamplin (Pergamon, Oxford, 1979), Vol. 2, p. 3; R. Dingle, *Festkörperprobleme,* edited by J. Treusch *(Advances in Solid State Physics)* (Pergamon, New York, 1975), Vol. 15, p. 21.

[2]J. N. Schulman and T. C. McGill, Phys. Rev. Lett. **39**, 1680 (1977).

[3]G. A. Sai-Halasz, R. Tsu, and L. Esaki, Appl. Phys. Lett. **30**, 651 (1977).

[4]E. Caruthers and P. J. Lin-Chung, Phys. Rev. B **17**, 2705 (1978).

[5]J. Ihm, P. K. Lam, and M. L. Cohen, Phys. Rev. B **20**, 4120 (1979).

[6]S. R. White and L. J. Sham, Phys. Rev. Lett. **47**, 879 (1981).

[7]G. Bastard, Phys. Rev. B **14**, 5693 (1981); **25**, 7584 (1982).

[8]J. N. Schulman and Y. C. Chang, Phys. Rev. B **24**, 4445 (1981).

[9]Y. C. Chang and J. N. Schulman, Appl. Phys. Lett. **43**, 536 (1983).

[10]G. A. Sai-Halasz, L. L. Chang, J.-M. Welter, C. A. Chang, and L. Esaki, Solid State Commun. **27**, 935 (1978).

[11]R. C. Miller, D. A. Kleinman, W. A. Nordland, Jr., and A. C. Gossard, Phys. Rev. B **22**, 863 (1980).

[12]C. Weisbuch, R. C. Miller, R. Dingle, A. C. Gossard, and W. Wiegman, Solid State Commun. **37**, 219 (1980).

[13]A. C. Gossard, in *Treatise on Material Science and Technology,* edited by K. T. Tu and R. Rosenberg (Academic, New York, 1982), p. 13.

[14]C. Colvard, R. Merlin, M. V. Klein, and A. C. Gossard, Phys. Rev. Lett. **45**, 298 (1980).

[15]J. N. Schulman and Y. C. Chang, preceding paper, Phys. Rev. B **31**, 2056 (1985).

[16]See, for example, F. Bassani and G. P. Parravicini, *Electronic States and Optical Transitions in Solids* (Pergamon, New York, 1975), Chap. 7.

[17]J. N. Schulman and Y. C. Chang, Phys. Rev. B **27**, 2346 (1983).

[18]M. Cardona and F. H. Pollak, Phys. Rev. **142**, 530 (1966).

[19]F. H. Pollack, C. W. Higginbotham, and M. Cardona, J. Phys. Soc. Jpn. **21**, Suppl. 20 (1966).

[20]J. M. Luttinger and W. Kohn, Phys. Rev. **97**, 869 (1956).

[21]G. D. Sanders and Y. C. Chang (unpublished).

[22]R. L. Greene and K. K. Bajaj, Solid State Commun. **45**, 831 (1983).

[23]M. S. Skolnick, A. K. Jain, R. A. Stradling, J. Leotin, J. C. Qusset, and S. Askenazy, J. Phys. C **9**, 2809 (1976).

[24]P. Lawaetz, Phys. Rev. B **4**, 3460 (1971).